ACS OMEGA

http://pubs.acs.org/journal/acsodf

Article

In Vitro and *In Silico* Characterization of Kurarinone as a Dopamine D_{1A} Receptor Antagonist and D_{2L} and D_4 Receptor Agonist

Ritu Prajapati, Su Hui Seong, Pradeep Paudel, Se Eun Park, Hyun Ah Jung,* and Jae Sue Choi*

Cite This: *ACS Omega* 2021, 6, 33443−33453

Read Online

ACCESS | Metrics & More | Article Recommendations | Supporting Information

ABSTRACT: Alterations in the expression and/or activity of brain G-protein-coupled receptors (GPCRs) such as dopamine D_1R, $D_{2L}R$, D_3R, and D_4R, vasopressin $V_{1A}R$, and serotonin 5-$HT_{1A}R$ are noted in various neurodegenerative diseases (NDDs). Since studies have indicated that flavonoids can target brain GPCRs and provide neuroprotection via inhibition of monoamine oxidases (hMAOs), our study explored the functional role of kurarinone, an abundant lavandulated flavonoid in *Sophora flavescens*, on dopamine receptor subtypes, $V_{1A}R$, 5-$HT_{1A}R$, and hMAOs. Radioligand binding assays revealed considerable binding of kurarinone on D_1R, $D_{2L}R$, and D_4R. Functional GPCR assays unfolded the compound's antagonist behavior on D_1R (IC_{50} 42.1 ± 0.35 μM) and agonist effect on $D_{2L}R$ and D_4R (EC_{50} 22.4 ± 3.46 and 71.3 ± 4.94 μM, respectively). Kurarinone was found to inhibit hMAO isoenzymes in a modest and nonspecific manner. Molecular docking displayed low binding energies during the intermolecular interactions of kurarinone with the key residues of the deep orthosteric binding pocket and the extracellular loops of D_1R, $D_{2L}R$, and D_4R, validating substantial binding affinities to these prime targets. With appreciable $D_{2L}R$ and D_4R agonism and D_1R antagonism, kurarinone might be a potential compound that can alleviate clinical symptoms of Parkinson's disease and other NDDs.

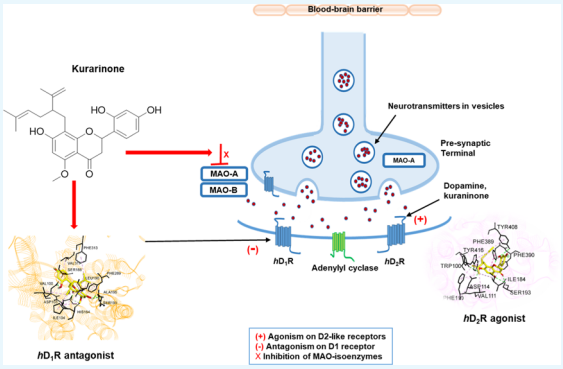

1. INTRODUCTION

G-protein-coupled receptors (GPCRs), also known as seven-transmembrane receptors, represent the largest set of cell membrane receptors that modulate a wide range of physiological functions and are emerging molecular targets in the drug development process. Different GPCRs have been linked to the pathophysiology of a variety of diseases including metabolic disorders (diabetes and obesity), immunological, cancer, cardiovascular, and neurodegenerative diseases (NDDs), and thus, they become potential drug targets for therapy.[1] Of 800 human GPCRs identified, over 90% of the nonsensory GPCRs occur in the central nervous system (CNS) and regulate mood, appetite, pain, immune system, cognition, and synaptic transmission. Alzheimer's disease (AD), vascular dementia, frontotemporal dementia, Parkinson's disease (PD), Huntington's disease (HD), and autism are common NDDs in which alterations in the GPCR expression and/or activity are observed in conjunction with neuropathological and clinical features such as cognitive and motor dysfunctions and neuropsychiatric illness.[2] Dopamine (DA), serotonin (5-HT), histamine, opioid, and adrenergic receptors are the established GPCR target families for the NDDs.[3]

DA is a major catecholaminergic neurotransmitter that participates in various neurological processes such as locomotor function, rewards, motivation, emotion, cognition, and neuroendocrine secretions. The actions of DA are mediated by five DA receptor (DAR) subtypes that are classified into two subclasses: $G\alpha_{s/olf}$-coupled D_1-like (D_1 and D_5) and $G\alpha_{i/o}$-coupled D_2-like (D_2, D_3, and D_4). Among the different subtypes, the human CNS shows the highest expression of D_1R followed by D_2R, while D_4Rs are minimally expressed. The perturbation of DA transmission and DAR activity lead to different pathological conditions such as PD, multiple sclerosis, schizophrenia, attention-deficit/hyperactivity disorder, Tourette syndrome, drug abuse, AD, and HD. Thus, DAR modulators (agonists and antagonists) find applications in the management of symptoms associated with these neurological illnesses.[4−6] Serotonergic 5-HT_{1A} receptors (5-$HT_{1A}Rs$), which are abundantly expressed in the hippocampus, were found to be reduced in the hippocampal fields and raphe nuclei, whereas an increase in 5-$HT_{1A}Rs$ at the caudal regions of striatum was observed in chronic parkinsonian monkeys.[7] Postmortem studies also revealed a decline in 5-$HT_{1A}Rs$ in the brains of AD patients.[8] Addition-

Received: August 2, 2021
Accepted: November 24, 2021
Published: December 6, 2021

ally, 5-HT_{1A}Rs are also implicated in the pathogenesis of anxiety and depression. Different studies indicate the significance of targeting 5-HT_{1A}Rs for ameliorating various motor (extrapyramidal disorders), mood (anxiety and depression), and nonmotor symptoms (impairment in learning and memory) in NDDs.[9] Thus, 5-HT_{1A}Rs are regarded as a therapeutic target for mitigating the symptoms of NDDs. Another GPCR target that plays a crucial role in learning and memory is a vasopressin V_{1A} receptor (V_{1A}R), which is widely distributed in the CNS (septum, cerebral cortex, hippocampus, and hypothalamus). Besides a fundamental role in fluid homeostasis and blood pressure regulation, arginine vasopressin (AVP), a neurohypophyseal peptide, plays a crucial role in social recognition, learning, memory, and anxiety-related behavior mediated via V_{1A}R. Studies conducted on vasopressin receptor (V_{1A}R) knockout mice reported a deficit of social recognition, impairment of spatial learning, and decreased anxiety-related behavior.[10,11]

Monoamines such as DA, 5-HT, epinephrine, and norepinephrine are the major GPCR ligands which are metabolized by monoamine oxidases (MAOs). Of the two isoforms, MAO-A is found primarily in catecholaminergic neurons of the locus coerulus, where it degrades 5-HT and norepinephrine. MAO-B is located in serotonergic neurons of the raphe nucleus and glial cells and selectively oxidizes phenylethylamine and benzylamine. Other brain bioamines such as DA, tyramine, and tryptamine are deaminated by both isoforms of MAOs. MAO-B accounts for about 80% of the overall MAO activity and major striatal DA oxidation compared to MAO-A. Both MAO-A and -B were found to be elevated in the postmortem brain of patients suffering from NDDs such as AD and PD. Therefore, the inhibitors of MAOs are used as an adjunct therapy in PD and AD, while the antidepressant action is associated with the inhibition of MAO-A.[12]

Sophora flavescens (Fabaceae) occurs as a wild and cultivated perennial shrub in Northeast Asia. The roots of *S. flavescens* (Kushen) represent an important component in the traditional Chinese medication and offer a rich source of prenylated flavonoids such as sophoraflavonone G, kurarinone, kurarinol, kushenol E, kushenol F, kuraridin, xanthohumol, and others that are known to possess antioxidant, anti-inflammatory, antidiabetic, cytotoxic, and MAO inhibitory activities.[13−15] Recently, these prenylated flavonoids have drawn attention to their potential role in NDDs owing to multiple reported bioactivities such as inhibition of β-site APP cleaving enzyme 1 (BACE 1), acetylcholinesterase (AChE), and butyrylcholinesterase (BChE);[16] suppression of MAO;[15] and protection of hippocampal cells against neurotoxic chemicals.[17] Kurarinone (Figure 1), a 2′,4′,7-trihydroxy-5-*O*-methoxy-8-lavandulated flavanone, is the most abundant flavonoid in *S. flavescens* radix[18] with a moderate to potent inhibitory action on BACE 1 (IC_{50}: 24.50 ± 1.73 μM), BChE (IC_{50}: 5.29 ± 0.67 μM), and AChE (IC_{50}: 74.28 ± 7.85 μM).[16] Kurarinone has shown a considerable reduction of CNS inflammation and demyelination and the suppression of the development of autoimmune encephalitis in a murine model of MS.[19] These observations suggest that kurarinone might have beneficial effects in NDDs, which involve multiple underlying causes. Additionally, an HPLC-based activity profiling study by Yang et al. identified kurarinone as a new scaffold with a flavonoid moiety possessing $GABA_A$ receptors modulating effect (EC_{50}: 8.1 ± 1.4 μM).[20] Studies have revealed that the DARs are involved in the modulation of $GABA_A$ receptors.[21,22] Thus, our present study aims to disentangle the modulatory activity of kurarinone on DA (D_1, D_2, D_3, and D_4) receptors and also on V_{1A} and $5HT_{1A}$ receptors, since these receptors are associated with pathophysiology of the CNS disorders. Receptor binding assays and GPCR functional assays were performed together with molecular docking studies to explore the pharmacological significance of kurarinone on the tested receptors. Additionally, we investigated the human recombinant MAO (hMAO) inhibition potential of kurarinone because previous studies have found that the prenylated flavonoids such as formononetin, kushenol F, and sophoraflavanone B inhibit MAO activity.[15,23]

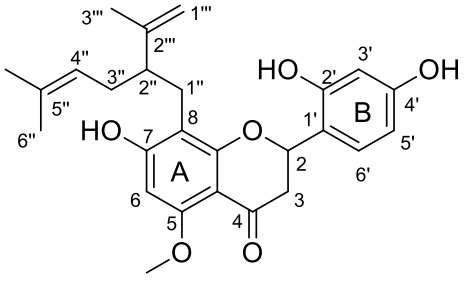

Figure 1. Chemical structure of kurarinone.

2. RESULTS

2.1. Binding Affinity of Kurarinone for Human DA and Vasopressin Receptors. Antagonist radioligand binding assays were carried out to examine the binding affinity of 50 μM kurarinone on DA D_1R, D_{2L}R, D_3R, and D_4R. V_{1A}R-binding property was determined by the agonist radioligand binding assay using [^{3}H]AVP on the recombinant CHO−V_{1A}R membrane homogenates. Table 1 presents the receptor-binding data of kurarinone. The percentage (%) inhibition of control-specific binding indicates the binding characteristic of the compound. Significant binding (>70%) by 50 μM kurarinone was observed on recombinant CHO-D_1R, HEK-D_{2L}R, and CHO-D_4R with the highest binding on CHO-D_1R (99.1% inhibition of control specific binding). No significant displacement of radioligands was observed from CHO-D_3R and CHO-V_{1A}R, which indicated a weak affinity of kurarinone for D_3R and V_{1A}R.

2.2. Functional Activity of Kurarinone on Human Recombinant D_1, D_{2L}, D_4, and $5HT_{1A}$ Receptors. Since a significant receptor-binding property of kurarinone was observed on D_1, D_{2L}, and D_4 receptors, the functional activities of kurarinone on these receptors were assessed. The agonist and antagonist effects of kurarinone on D_1 and D_4 receptors were evaluated using the cAMP assay, while the activity on the D_{2L} receptor was examined using calcium (Ca^{2+}) flux assay on transfected CHO cells. We also evaluated the effect of the compound on intracellular Ca^{2+} ion mobilization on recombinant Ba/F3-5-HT_{1A}R cells to determine modulatory function on 5-HT_{1A}R because many DAR agonists, which were approved as anti-Parkinson agents, are known to interact with this receptor and have an influence on motor function, mood, and cognition.[24] The results of the agonist and antagonist cell-based functional assays showing the functional effect and efficacy of kurarinone on the tested receptors are summarized in Table 2. The agonist effect of kurarinone is presented by the % stimulation of control agonist response, while antagonist

https://doi.org/10.1021/acsomega.1c04109
ACS Omega 2021, 6, 33443−33453

Table 1. DA D_1, D_2, D_3, and D_4 and Vasopressin V_{1A} Receptor-Binding Data of Kurarinone

receptors	radioligand	% inhibition of control-specific binding[a] (%)	reference antagonist	reference IC_{50}[b]
D_1	[^{3}H]SCH-23390	99.1	SCH23390	0.5
D_{2L}	[^{3}H]methylspiperone	78.5	(+)butaclamol	2.6
D_3	[^{3}H]methylspiperone	49.2	(+)butaclamol	4.6
D_4	[^{3}H]methylspiperone	71.1	(+)butaclamol	93
V_{1A}[c]	[^{3}H]AVP	47.6	[d(CH_2)$_5^1$,Tyr(Me)$_2$]-AVP	1.4

[a]Values are presented as the mean of percent inhibition of control-specific binding by 50 μM kurarinone performed in duplicate. [b]Concentration producing 50% inhibition of the control-specific binding by the reference antagonists (nM). [c]Agonist radioligand binding assay.

Table 2. Functional Effect (% Stimulation and % Inhibition) and Efficacy (EC_{50} and IC_{50}) of Kurarinone on Human DA (hD_1, hD_{2L}, and hD_4) and Serotonin ($h5\text{-}HT_{1A}$) Receptors

receptors	% stimulation[a] (% inhibition)[b]	EC_{50}[c] (IC_{50})[d]	reference agonist[e] (reference antagonist)[f]	reference EC_{50}[g] (IC_{50})[h]
hD_1	0.25 ± 0.64^D (98.5 ± 1.48)^C	42.1 ± 0.35	DA (SCH-23390)	44 (1.3)
hD_2L	113 ± 28.9^B (43.8 ± 25.9)^C AGO	22.4 ± 3.46	DA (butaclamol)	31 (26)
hD_4	71.7 ± 6.36^C (−4.20 ± 2.55)^D	71.3 ± 4.94	DA (clozapine)	13 (520)
$h5\text{-}HT_{1A}$	17.8 ± 1.13^D (30.3 ± 6.58)^C		serotonin ((S)-WAY-100635)	2.9 (7.0)

[a]% stimulation represent % stimulation of control agonist effect, by kurarinone at 100 μM. [b]% inhibition represent % inhibition of control agonist effect, by kurarinone at 100 μM. [c]Concentration required to exhibit 50% of control agonist effect (μM). [d]Concentration required to inhibit 50% of control agonist effect (μM). Values denoted as mean ± S.D. from a duplicate experiment. [e]Reference agonists for each assay. [f]Reference antagonists for each assay. [g]EC_{50} of the reference agonist (nM). [h]IC_{50} of the reference antagonist (nM). AGO: the test compound induced at least 25% agonist or agonist-like effect at this concentration. [B−D]Different letters indicate a significant difference of kurarinone's effect on different receptors ($p < 0.05$, Duncan's test). (−) Not tested.

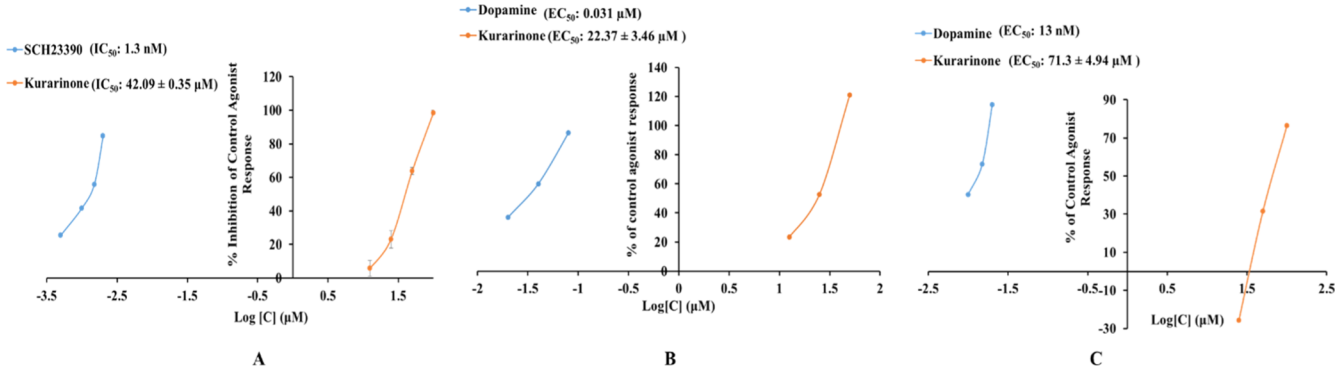

Figure 2. Concentration-dependent percentage inhibition of control agonist response of kurarinone on hD_1R (A). Concentration-dependent percentage of control agonist response of kurarinone on hD_2R (B) and hD_4R (C).

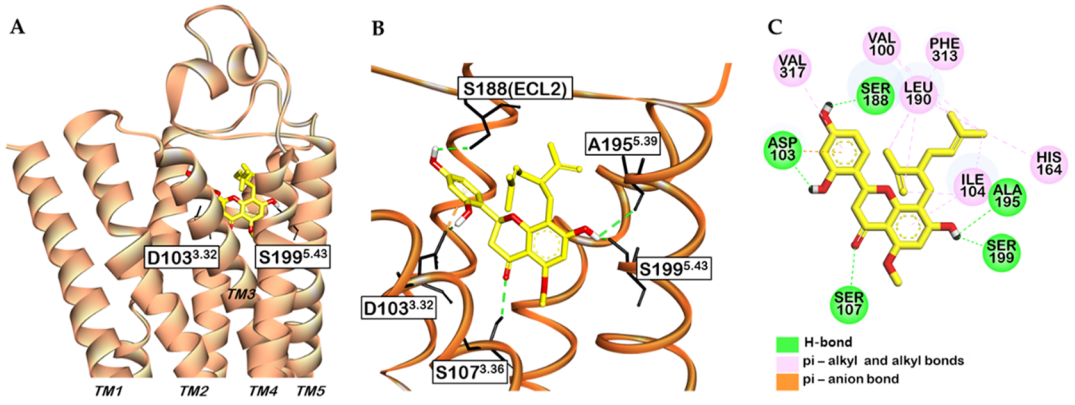

Figure 3. Molecular docking of kurarinone (yellow stick) to the hD_1R model (A). Zoom-in view of the ligand-binding pocket of the hD_1R model in complex with kurarinone obtained from docking simulation (B). The superscript refers to the Ballesteros−Weinstein numbering system for GPCR. Two-dimensional representation of the binding mode of kurarinone with key amino acid residues of hD_1R (C).

behavior is indicated by % inhibition of control agonist response.[25] On preliminary screening of functional activity, 100 μM kurarinone showed notable agonist response on $D_{2L}R$ and D_4R with % stimulation of a control agonist response of 113 ± 28.9 and 71.7 ± 6.36%, respectively. It had a negligible agonist effect on D_1R and $5HT_{1A}R$. In the antagonist mode

https://doi.org/10.1021/acsomega.1c04109
ACS Omega 2021, 6, 33443−33453

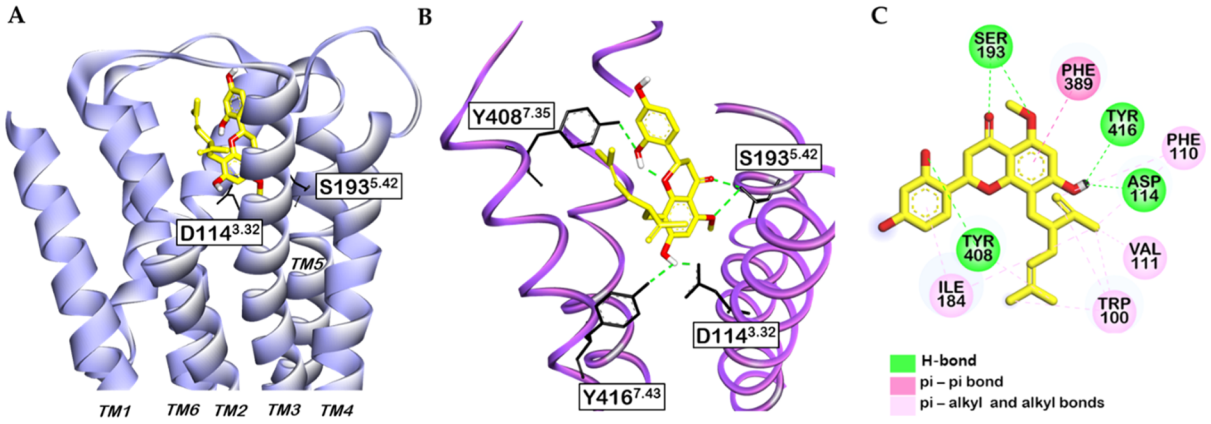

Figure 4. Molecular docking of kurarinone (yellow stick) to the $hD_{2L}R$ model (A). Zoom-in view of the ligand-binding pocket of the $hD_{2L}R$ model in complex with kurarinone obtained from docking simulation (B). The superscript refers to the Ballesteros−Weinstein numbering system for GPCR. Two-dimensional representation of the binding mode of kurarinone with key amino acid residues of $hD_{2L}R$ (C).

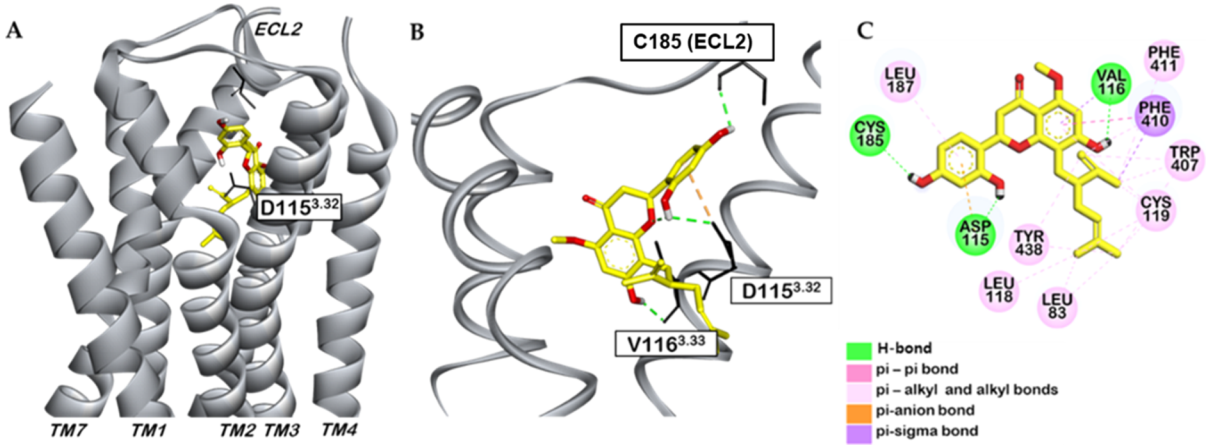

Figure 5. Molecular docking of kurarinone (yellow stick) to the hD_4R model (A). Zoom-in view of the ligand-binding pocket of the hD_4R model in complex with kurarinone obtained from docking simulation (B). The superscript refers to the Ballesteros−Weinstein numbering system for GPCR. Two-dimensional representation of the binding mode of kurarinone with key amino acid residues of hD_4R (C).

assays, 100 μM kurarinone displayed a significant effect on D_1R with the % inhibition of control agonist response of 98.5 ± 1.48%. On $D_{2L}R$, it showed 43.8 ± 25.9% antagonist effect but with at least 25% agonist response. Thus, kurarinone cannot produce full antagonist response and results in an apparent inhibition only. Similarly, 100 μM compound inhibited the maximal control agonist response on $5HT_{1A}R$ moderately with 30.3 ± 6.58% inhibition and had no antagonist effect on D_4R. From these observations, kurarinone is detected to have a significant D_1R antagonist effect and a $D_{2L}R$ and D_4R agonist effect, measured at 100 μM.

Further functional evaluations were made using lower concentrations of kurarinone on D_1, D_{2L}, and D_4 receptors which revealed its dose-dependent antagonist activity on D_1R with an IC_{50} of 42.1 ± 0.35 μM and dose-dependent agonist effects on $D_{2L}R$ and D_4R with an EC_{50} of 22.4 ± 3.46 and 71.3 ± 4.94 μM, respectively. Figure 2 shows the concentration-dependent modulatory effects of kurarinone on DAR subtypes along with the corresponding EC_{50} and IC_{50} values.

2.3. Molecular Docking of Kurarinone with DA D_1, D_{2L}, and D_4 Receptors. To understand the interactions of kurarinone within the active sites of D_1R, $D_{2L}R$, and D_4R, we conducted computational docking studies using the homology model for human D_1R and the crystallographic structures of 6CM4 and 5WIV for $hD_{2L}R$ and hD_4R, respectively. The binding energies and the ligand−receptor interactions obtained from the *in silico* analysis are tabulated in Table S1. The best docking poses (with the lowest binding energy) obtained for the kurarinone−hD_1R, $hD_{2L}R$, and hD_4R complexes, along with the corresponding ligand−protein interactions, are shown in Figures 3−5, respectively.

Probing the ligand−receptor interactions with the hD_1R model revealed that kurarinone is located within the ligand-binding site between the transmembranes (TMs) 3, 4, 5, and 7 with a good binding affinity (−6.96 kcal/mol, which is comparable to that of the selective hD_1R antagonist SCH-23390 having binding energy −7.16 kcal/mol). Kurarinone fitted into the binding pocket of the receptor by interacting with conserved binding site amino acid residues such as $Val100^{3.29}$, $Ile104^{3.33}$, $His164^{4.66}$, $Ala195^{5.39}$, $Phe313^{7.35}$, and $Val317^{7.39}$ through hydrophobic bonds. Extracellular loops (ECLs) are considered important in defining the ligand-binding site of any particular receptor. The docking result (Figure 3) displayed the hydrophobic interaction of kurarinone with Leu190 and polar binding with Ser188 of ECL_2. Unlike the π−cation interaction observed with agonist DA, kurarinone was predicted to have an electrostatic link with an important binding site residue $Asp103^{3.32}$ of hD_1R via a π−anion bond.

https://doi.org/10.1021/acsomega.1c04109
ACS Omega 2021, 6, 33443−33453

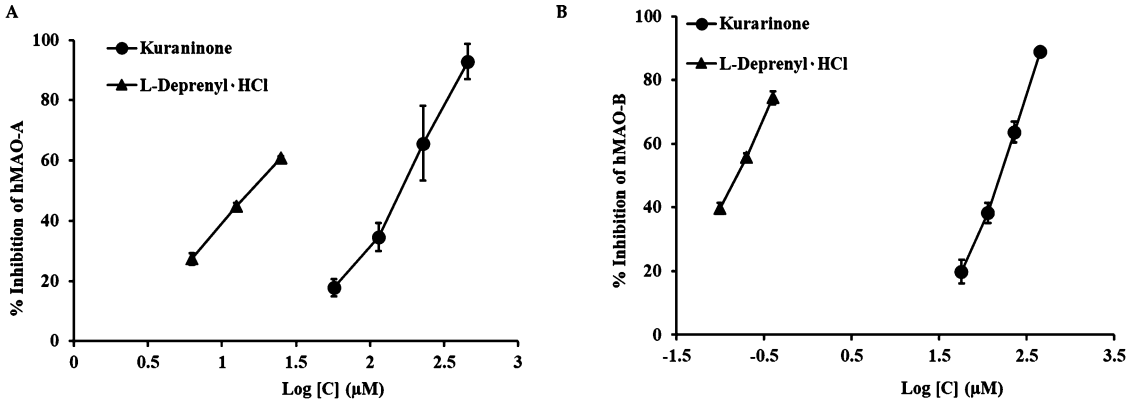

Figure 6. Dose-dependent inhibition of hMAO-A (A) and hMAO-B (B) by kurarinone and L-deprenyl·HCl.

Additional H-bonding occurred with Asp103$^{3.32}$, Ser107$^{3.36}$, Ala195$^{5.39}$, and Ser199$^{5.43}$.

The docking study on DA $hD_{2L}R$ demonstrated that the chroman-4-one moiety of kurarinone was located in the deep binding pocket within the TMs 3, 5, and 6, interacting with Asp114$^{3.32}$, Val111$^{3.29}$, Phe110$^{3.28}$, Ser193$^{5.42}$, Phe390$^{6.51}$, and Phe389$^{6.51}$ through hydrophilic and hydrophobic mechanisms via different bonds, as shown in Figure 4C, whereas the dihydroxyphenyl and lavandulyl or 8-(5-methyl-2-prop-1-en-2-ylhex-4-enyl) substituents extended toward the extracellular part of TM7 and interacted with the residues defining hD_{2L}-extended binding pocket (D_{2L}-EBP) such as Trp110 (ECL_1), Ile184 (ECL_2), and Tyr408$^{7.35}$ and Tyr416$^{7.43}$ (TM_7) via both H-bonds and nonpolar interactions. These interactions might have resulted in high affinity binding of kurarinone to the $hD_{2L}R$ (−7.46 kcal/mol). In our experiment, reference agonist (DA) and antagonist (butaclamol) did not engage with the ECL residues (Table S1).

As shown in Figure 5, the molecular docking of kurarinone with hD_4R presented a lower binding energy of −7.61 kcal/mol (strong binding) in comparison with DA but a higher energy requirement compared to the D_4R antagonist, nemonapride (−10.5 kcal/mol). For D_4R modulatory activity, specific interaction with a highly conserved residue Asp115$^{3.32}$ through hydrophilic interactions such as a salt bridge and −OH bond was identified vital using agonist DA and antagonist nemonapride. Kurarinone displayed binding with Asp115$^{3.32}$ through H-bonding and electrostatic interactions through the 2′-OH group and the phenyl ring B, respectively. The lavandulyl substituent together with the 7-hydroxy-5-methoxychromen-4-one ring of kurarinone exhibited hydrophobic interactions with conserved orthosteric binding pocket (OBP) lined by residues such as Leu83$^{2.53}$, Val116$^{3.33}$, Leu118$^{3.35}$, Cys119$^{3.36}$, Trp407$^{6.48}$, Phe410$^{6.51}$, Phe411$^{6.52}$, and Tyr438$^{7.43}$. Additionally, the 2,4-dihyroxyphenyl moiety extended to bind with extracellular conserved residues Cys185 and Leu187 of ECL_2 via H-bonding and π−alkyl interaction with the 4′-OH group and phenyl ring B, respectively.

2.4. hMAO Inhibition by Kurarinone. Recombinant human MAO inhibitory activity of kurarinone was studied using a chemiluminescent assay in a 96-well opaque white plate using an MAO-Glo kit. On testing the compound at different concentrations (456, 228, 114, and 57 μM) against hMAO-A and hMAO-B, dose-dependent inhibition was observed, as shown in Figure 6. Kurarinone exhibited a very weak inhibitory effect on both hMAO-A and hMAO-B with IC_{50} values of 186 ± 6.17 and 198 ± 12.66 μM, respectively (Table 3). In the kinetic analyses, kurarinone showed competitive inhibition of hMAO-A with K_i values of 65.1 ± 3.53 μM, whereas it showed mixed inhibition of hMAO-B (Table S2). From secondary plots, the inhibition constant with a free enzyme (K_{ic}) was determined to be 12.3 ± 2.41 μM and that with an enzyme−substrate complex (K_{iu}) was 144 ± 4.21 μM. The double reciprocal Lineweaver−Burk plots and Dixon and secondary plots obtained from the kinetic data are shown in Figure S1.

Table 3. Recombinant hMAO Inhibitory Activity of Kurarinone and the Reference Drug

	hMAO-A	hMAO-B	
compound	IC_{50} [a]	IC_{50} [a]	SI[b]
kurarinone	186 ± 6.17	198 ± 12.7	0.94
l-deprenyl·HCl[c]	15.6 ± 0.67	0.17 ± 0.01	91.94

[a]The 50% inhibitory concentration (IC_{50}) values (μM) were calculated from a log dose inhibition curve and expressed as the mean ± SD of triplicate experiments. [b]The selectivity index (SI) was determined as the ratio of IC_{50} for hMAO-A inhibition to IC_{50} for hMAO-B inhibition. [c]Positive control, expressed as μM.

A molecular docking study was conducted to elucidate the binding mode and interactions between kurarinone and hMAO isoenzymes using AutoDock 4.2. The docking study revealed that kurarinone could pose within the active site of hMAO-A with a binding energy of −10.72 kcal/mol and interact with the cofactor FAD600 and the active site residues such as Tyr444, Phe208, Tyr407, Ile335, Leu337, Met350, Phe352, Ile180, Ser209, Thr336, and Glu216 via different kinds of interactions such as hydrophobic, H-bonding, and electrostatic interactions (Table S3 and Figure S2). From the computational docking, it was found that kurarinone can interact with both catalytic and allosteric binding site residues of hMAO-B with low binding energies of −11.88 and −9.82 kcal/mol, respectively (Table S3 and Figure S3). Despite low binding energies required to stabilize kurarinone−hMAO complexes, kurarinone was only a modest inhibitor of hMAO-A and hMAO-B. It has been known that the aromatic interactions with catalytic site tyrosine residues (Tyr407 and Tyr444 of hMAO-A and Tyr398 and Tyr435 of hMAO-B) and cofactor FAD are important for the strong substrate/inhibitor binding. Also, the amino acids Phe208 (Ile119 in hMAO-B) and Ile335 (Tyr326 in hMAO-B) of the active site of hMAO-A are critical for substrate selectivity.[26−28] Although kurarinone can interact with multiple active site residues, hydrophobic π−π

https://doi.org/10.1021/acsomega.1c04109
ACS Omega 2021, 6, 33443−33453

Table 4. *In Silico* Prediction of Drug-Likeliness, ADME Characteristics, and Toxicity of Kurarinone

	drug-likeliness		ADME characteristics						toxicity
compound	MDDR-like rule	Lipinski's rule	log $P_{o/w}$[a]	PPB[b]	HIA[c]	MDCK cell permeability (nm/s)[d]	Caco2 permeability (nm/s)[e]	BBB penetration ([brain]/[blood])[f]	Ames test
kurarinone	drug-like	suitable	5.55	99.3	92.3	0.05	22.9	4.02	non-mutagen

[a]Lipophilicity represented by the *n*-octanol−water partition coefficient. [b]Plasma protein binding (<90% denotes weak binding and >90% denotes strong binding). [c]Human intestinal absorption (0−20%: poorly absorbed; 20−70%: moderately absorbed; and 70−100% is well-absorbed). [d]Permeability across Madin−Darby canine kidney (MDCK) cells. [e]Permeability across human colorectal adenocarcinoma cells (0−10: low permeability; 10−100: medium permeability; and >100: high permeability). Permeability across the BBB (<0.1: low absorption; 0.1−2.0: middle absorption; and >2.0: high absorption).

interactions with the aromatic rings of critical catalytic tyrosine residues were missing in the complexes of kurarinone and hMAO-A/B.

2.5. *In Silico* Prediction of Drug-Likeliness and ADME.

Table 4 presents the pharmacokinetic parameters assessed for kurarinone using the PreADMET application. Kurarinone followed Lipinski's rule of five, thus indicating suitability for oral administration.[29] Also, it fitted to the MDDR-like rule and was found to have drug-like characteristics. The log Po/w value was anticipated to be 5.5 for the test compound. Kurarinone exhibited >90% of plasma protein binding and high intestinal absorption (>70%). Permeability across Coca-2 and MDCK cells was expected to be 0.05 and 22.93 nm/s, respectively. For molecules targeting the CNS, they should pass readily through the blood−brain barrier (BBB). Kurarinone was estimated to have high permeability across the BBB as the ratio of concentration in the brain relative to the blood was 4.02. Overall, PreADMET results indicated kurarinone as a suitable candidate for drug development with the nonmutagenic property. However, these predicted results can vary from the experimental values.

3. DISCUSSION

Over the past decade, different flavonoids have been identified with a potential role in NDDs through multiple mechanisms such as anti-inflammatory, antioxidant, and anti-apoptosis.[30] Experimental and clinical studies provide evidence on the improvement of cognition and learning by flavonoids through the modulation of neuronal signaling pathways, facilitating neurogenesis and inhibiting neurodegeneration and neuroinflammation.[31−33] Nevertheless, research on the modulatory activity of flavonoids on GPCRs is limited.[34] In our previous work, we reported luteolin, a 3′,4′,5,7-tetrahydroxyflavone, to be a selective antagonist of $V_{1A}R$ and D_4R and a selective hMAO-A inhibitor.[35] Our present study found that kurarinone at 50 μM could significantly bind to the hD_1R, $hD_{2L}R$, and hD_4R in the order of $hD_1R > hD_{2L}R > hD_4R$. From the GPCR functional assay, kurarinone was identified to have an $hD_{2L}R$ agonist effect (EC_{50} 22.4 ± 3.46 μM) and an antagonist effect on hD_1R (IC_{50} 42.1 ± 0.35 μM). It also displayed substantial binding to hD_4R and stimulated the receptor with an EC_{50} of 71.3 ± 4.94 μM. No significant binding and activity were observed on $5HT_{1A}R$ and $V_{1A}R$.

In silico docking was performed to understand the molecular interactions of kurarinone at the active sites of the hD_1R, $hD_{2L}R$, and hD_4R. The molecular docking of DA with the hD_1R model detected the H-bond formation between the aromatic hydroxyl groups of DA and Asp103$^{3.32}$ (salt bridge), Ser202$^{5.46}$, Ser198$^{5.42}$, and Ser199$^{5.43}$. Investigation of binding modes of D_1-selective antagonist SCH23390 (R) to the model revealed H-bond interaction with Asp103$^{3.32}$, Ala195$^{5.39}$, and Ser199$^{5.43}$, which were also present with the kurarinone−receptor association. Binding to Ser199$^{5.43}$ of TM_5 and Ser107$^{3.36}$ (TM_3), as well as to TM_7 residues, has been reported liable for the higher binding affinities of D_1R antagonists to the receptor.[36,37] These molecular interactions might account for the notable antagonist behavior of kurarinone on hD_1R. Likewise, kurarinone displayed interactions with the defined residues of D_{2L}-EBP in addition to that with the reactive loci of binding sites in $D_{2L}R$. These interactions were similar to those observed with the inverse agonist risperidone−D_2R complex.[38] Generally, DA D_2R agonists bind tightly with serine residues Ser193$^{5.42}$ and Ser194$^{5.43}$ of TM_5 via H-bonds together with Asp114$^{3.32}$ in TM_3 via salt bridge formation.[39] These findings are consistent with the interaction observable in D_{2L}−kurarinone binding, as the compound is anchored with Ser193$^{5.42}$ and Asp114$^{3.32}$ by H-bonds. Moreover, the $D_{2L}R$ binding was stabilized by alkyl and π-alkyl interactions with the highly conserved hydrophobic residue of ECL_2, Ile184.[38] *In silico* docking revealed that kurarinone binds to the conserved OPB and EBP residues of hD_4R. Interactions of the compound with hD_4R OPB residues such as Asp115$^{3.32}$, Val116$^{3.33}$, Cys119$^{3.36}$, and Phe411$^{6.52}$ are common to those found in the complexes of reference ligands (DA and nemonapride) and hD_4R.

Even though earlier studies have reported hMAO inhibition potential of some prenylated flavonoids from *S. flavescens*, the ability of kurarinone to act on hMAO was unknown.[15,23] Thus, we examined the activity of kurarinone on hMAO-A and hMAO-B and observed a modest and nonselective inhibition of hMAO isoenzymes. Formerly, a structurally similar flavanone but devoid of a 5-*O*-methoxy substituent, sophoraflavone G, had displayed selective hMAO-A inhibition with an IC_{50} value of 38.8 ± 1.1 μM.[23] The docking study demonstrated that the lavundulyl substituent in the structure of kurarinone facilitated most of the hydrophobic interactions with the enzymes. However, the weak activity of the compound might be due to the hindrance by the same moiety to make aromatic sandwich interactions between the aromatic rings of kurarinone with the catalytic recognition sites of the enzymes (Tyr residues and FAD).

DAR modulators have been implicated under different neurological conditions that involve abnormalities in dopaminergic (DAergic) transmission and its receptors. For instance, the loss of DAergic neurons resulting in a reduced level of DA in basal ganglia is the pathophysiological abnormality of PD, and to treat this condition, DAR agonists and DA precursor L-dopa are used to compensate for the loss or lack of endogenously produced DA,[5] whereas DAR antagonists are implicated in schizophrenia, where hyperactivation of the DAergic system occurs in mesolimbic pathways.[40]

https://doi.org/10.1021/acsomega.1c04109
ACS Omega 2021, 6, 33443−33453

PD is characterized by progressive damage to the nigrostriatal DAergic neurons involving reactive oxygen radical-mediated and iron-dependent lipid peroxidation that eventually leads to ischemia-induced brain injury. D_2 receptor agonists such as pramipexole, bromocryptine, lisuride, pergolide, and ropinirole afforded prominent protection against neurotoxin-induced cell apoptosis.[41−43] Likewise, D_2/D_3R agonist and 7-hydroxy-*N*,*N*-di-*n*-propyl-2-aminotetralin (7-OH-DPAT) induced significant neurogenesis in the SNc of the adult rat brain along with the betterment of locomotor function and enhanced reward learning.[44,45] Stimulation of D_4R has been related to novelty-seeking character, memory consolidation, and the striatal motor process.[46−48] A recent systematic review and meta-analysis by Pan and colleagues reported that the DA level was considerably lowered in AD patients along with the decrease in the levels of DARs. Clinical studies engaging pharmacological intervention by L-dopa and DAR agonists in AD patients have found improvement of cognitive ability and cortical plasticity.[49] Therefore, the benefits of DAR modulators and DA replacement therapy are not limited to PD.

D_1R activation induces cAMP-dependent activation of protein kinase (PKA) and increases the level of intracellular calcium (Ca^{2+}) levels via opening of L-type calcium channels. Lebel and colleagues reported that the D_1R activation-induced physiological changes mediate phosphorylation of tau proteins. Their study also showed that neither the D_2R agonism nor the reduction of cAMP levels affects tau-phosphorylation and cellular damage.[50] These observations suggest that kurarinone might play a plausible role in AD and other dementia via D_1R antagonism, as tau-hyperphosphorylation has been known to cause neuronal dysfunction and implicated in AD pathogenesis. D_1R stimulation has been implicated to cause oxidative stress and apoptosis through ERK activation. Indirect agonists such as cocaine and amphetamine augment the expression of D_1R-driven genes such as c-fos, c-Jun, phospho-cAMP response element-binding protein, and p-Elk-1, and such changes were inhibited by the pretreatment of the D_1R antagonist, SCH23390.[51] Moreover, SCH23390 also blocked the neurotoxicity caused by DA-induced D_1R signaling and autoxidation.[52] Increased D_1R signaling has also been associated in the pathogenesis of L-dopa-induced dyskinesia (LID) by different preclinical studies.[53−55] Grondin et al. reported that selective D_1R blockade reduces LID and, however, aggravates parkinsonism in parkinsonian monkeys.[56]

ADMET assessment by PreADMET predicted kurarinone to be a drug-like molecule capable of crossing the BBB (>4) (Table 4). Corroborating with the *in silico* prediction, previous *in vivo* studies have demonstrated high absorption and clearance and moderate bioavailability of kurarinone.[57,58] Despite a favorable ADME profile, Jiang et al.[59] and Yu et al.[60] in independent studies have detected kurarinone as a hepatotoxic compound in the *S. flavescens* extract owing to the hepatic accumulation of the compound and inhibition of fatty acid β-oxidation, resulting in lipid accumulation in the liver. In contrast, another study by Nishikawa and colleagues found the induction of heme oxygenase-1 by kurarinone via activation of the KEAP1/Nrf2 pathway and Nrf2 activation plays a protective role against hepatotoxicity.[61] The metabolic study suggests that glucuronidation plays a vital role in detoxification by the formation of soluble compounds that can be eliminated readily from the body. High hepatic accumulation and toxicity of kurarinone may result when the activity of UDP-glucuronosyltransferase is limited and high concentrations of kurarinone occur in the liver.[62] Studies on the mechanism of hepatic injury by kurarinone and the possible derivatization of the compound to generate functional derivatives with reduced hepatotoxicity may be important to establish kurarinone as a suitable drug-like molecule for the treatment of different diseases.

4. CONCLUSIONS

Our study evaluates DARs, V_{1A}R, and 5-HT_{1A}R modulatory activities and hMAO inhibition capacities of kurarinone for the first time. The knowledge of the pharmacological importance of flavonoids on GCPR modulation is scarce. Functional GPCR screening showed that kurarinone possessed D_{2L}R and D_4R agonist properties along with the ability to fully antagonize D_1R. For multifactorial complexities associated with NDDs such as AD and PD, molecules with a multitarget nature and minimal toxicity are anticipated to be potential therapeutics.[63] Thus, multifunctional nature of kurarinone might be beneficial for targeting different underlying causes of NDDs and ameliorating the associated symptoms. Further *in vivo* studies are necessary to support the *in vitro* DAR modulatory effects and observe the efficacy of kurarinone in alleviating DAergic neurodegeneration and disease conditions in animal models.

5. MATERIALS AND METHODS

5.1. Chemicals and Reagents. Kurarinone was isolated from the ethyl acetate fraction of *S. flavescens* radix as reported in our earlier work.[16] Recombinant Chinese hamster ovary (CHO) and human embryonic kidney (HEK-293) cells were generated by Eurofins Discovery (Le Bois I′ Eveque, France). ThermoFisher Scientific (Madison, U.S.A.) provided cell-culture media such as Roswell Park Memorial Institute (RPMI-1641), Dulbecco's modified Eagle medium buffer, Hank's balanced salt solution (HBSS) buffer, and 4-(2-hydroxyethyl)-1-piperazineethanesulfonic acid (HEPES) buffer. The MAO-A/B assay kit was acquired from Promega (Promega Cooperation, Madison, WI). The recombinant hMAO isoenzymes and the reference drugs: L-deprenyl·HCl, DA, 5-HT, AVP, clozapine, (+) butaclamol, SCH 23390, (S)-WAY-100635, and [$d(CH_2)_5^1$, $Tyr(Me)_2$]-AVP were supplied by Sigma-Aldrich (St. Louis, MO, USA). The remaining chemicals of reagent grade were procured from commercial suppliers.

5.2. Radioligand Binding Assays. The binding affinity of kurarinone to the membrane cloned with human DA and vasopressin receptors was characterized by the radioligand binding assays following the validated methods and standard procedures developed at the Eurofins Cerep (Le Bois I′ Eveque, France). The experimental methods for the binding assays were similar as described by Chen et al. and Gorbunov et al.[64,65] Human D_1R, D_3R, D_4R, and V_{1A}R binding was assessed using the membrane homogenates of the transfected CHO cells. For D_1, D_3, and D_4 receptors, the respective membrane homogenates were suspended in buffer solution comprising 50 mM Tris−HCl (pH 7.4), 5 mM KCl, 5 mM $CaCl_2$/120 mM NaCl, and 5 mM EDTA and incubated with 0.3 nM appropriate radioligands, [^{3}H] SCH23390 (for D_1R) and [^{3}H] methylspiperone (for D_3R and D_4R), at 22 °C for 1 h in the presence or absence of test compounds. In the case of V_{1A}R binding, the membrane homogenates were diluted in a

https://doi.org/10.1021/acsomega.1c04109
ACS Omega 2021, 6, 33443−33453

binding buffer consisting of 50 mM Tris−HCl (pH 7.4), 5 mM $MgCl_2$, and 0.1% BSA and incubated with [^{3}H] AVP at 22 °C for 1 h. $D_{2L}R$ binding was evaluated using the plasma membrane homogenates from the transfected HEK-293 cells. The membrane homogenates of $D_{2L}R$ expressing HEK-293 cells were suspended in binding buffer (50 mM Tris−HCl, 5 mM MgCl2, 1UI/mL ADA, 1 mM EDTA, 1 μg/mL leuleptin, 1 μM pepstatin, and 10 μg/mL trypsin inhibitor, pH 7.4) and incubated with 0.3 nM [^{3}H] methylspiperone for 1 h at 22 °C. 1 μM SCH23390 (for D_1R), 10 μM (+) butaclamol (for $D_{2L}R$, D_3R and D_4R), and 1 μM AVP (for $V_{1A}R$) were used to determine the nonspecific binding in the respective binding assays.

Radioligand binding within the reaction systems was ceased by filtration over 0.3% polyethyleneimine-treated glass fiber filters (GF/B, Packard). The filters were then rinsed multiple times with ice-cold wash buffer (50 mM Tris−HCl) using a 96-sample cell harvester (Unifilter, Packard) and dried. The dried filters were added with scintillation cocktail (Microscint O, Packard) and radioactivity was measured using a scintillation counter (Topcount, Packard). The binding property of the compound was computed as the percentage inhibition of control-specific binding. In each of the radioligand binding experiment, standard reference compounds were tested at different concentrations to obtain a competition curve from which their IC_{50} were derived.

5.3. *In Vitro* Functional GPCR Assay. GPCR functional assays were conducted at Eurofins Cerep (France) following the assay protocols in the experimental conditions as described earlier.[35,66] CHO cells stably expressing D_1R, D_2R, D_4R, and Ba/F3 cells transfected with $5HT_{1A}R$ were used to determine the modulatory effects of kurarinone, based on the measurement of the cAMP level (for D_1 and D_4 receptors) and calcium ion mobilization (for D_{2L} and HT_{1A} receptors).

5.3.1. Measurement of the cAMP Level. Recombinant CHO-D_1R and CHO-D_4R cells were suspended in HBSS buffer, supplemented with 20 mM HEPES buffer and 500 μM IBMX. The resulting cell suspension was seeded into cell plates at a density of 5×10^3 cells/well and incubated for 10−30 min with/without kurarinone or reference at RT (for CHO-D_1R suspension) or 37 °C (CHO-D_4R cell suspension). D_2-labeled cAMP conjugate and europium cryptate-labeled anti-cAMP antibody were distributed into the cell plate followed by the addition of lysis buffer and subsequent incubation for the next 1 h. Homogeneous time-resolved fluorescence (HTRF) readings were then obtained using an Envision microplate reader (PerkinElmer, Waltham, MA, USA) at an excitation intensity of 337 nm and emission intensities 620 and 665 nm. The results of the experiments were expressed as a percent of control agonist response (for agonist behavior) and as a percent inhibition of control agonist response (for antagonist behavior). Control stimuli used to calculate agonist effects of kurarinone on D_1R and D_4R were 10 μM and 1000 nm DA, respectively. Likewise, control stimuli used to measure the antagonist effect were 300 nm DA (for D_1R) and 100 nm DA (for D_4R).

5.3.2. Measurement of the Intracellular Calcium Level. The functional role of kurarinone on transfected CHO-$D_{2L}R$ and Ba/F3-5-$HT_{1A}R$ was assessed by measuring Ca^{2+} ion influx fluorimetrically. Transfected cells were diluted in HBSS/20 mM HEPES buffer (pH 7.4) and distributed into microplate wells at a density of 1×10^5 cells/well. To each well, a fluorescent probe (Fluo8 Direct, Invitrogen, Carlsbad, CA, USA) blended with probenecid in HBSS/20 M HEPES (pH 7.4) was added and incubated for 1 h at 37 °C. The fluorescence was then recorded after keeping the assay plate in a CellLux microplate reader (PerkinElmer, Waltham, MA, USA) and adding the sample or reference. The cellular agonist effect was obtained as the percentage of control response to 10 μM DA for $D_{2L}R$ and 0.625 μM 5-HT for 5-$HT_{1A}R$. Percentage inhibition of control response relative to 70 nM DA for $D_{2L}R$ and 15 nm 5-HT for 5-$HT_{1A}R$ was calculated to determine antagonist behavior.

5.4. Human Monoamine Oxidase-A and -B Inhibitory Assay and Enzyme Kinetics. The hMAO-A and -B inhibition potential of kurarinone was examined using an MAO-Glo assay kit in an opaque white 96-well plate following the manufacturer's protocol as described in our earlier report.[67] This assay is based on measuring luminescence produced by luciferin at the end of the reaction of the enzyme with substrates and test samples. Briefly, the initial reaction system in each well of the plate consisted of 12.5 μL of substrate (beetle luciferin derivative, 40 and 4 μM for hMAO-A and hMAO-B, respectively), 12.5 μL of kurarinone or L-deprenyl solutions (of varying concentrations), and 25 μL of enzyme solution. The mixture was let to equilibrate for 1 h at 25 °C. Following incubation, the enzyme reaction was ceased by adding 50 μL of luciferin detection reagent. The reaction plate was incubated for an extra 20 min at 25 °C, and luminescence from the plate was measured using a FilterMax F5 Multimode Microplate Reader (Molecular Devices, Sunnyvale, CA, USA).

An enzyme kinetics experiment was performed using different concentrations of the hMAO substrate (80 to 240 μM for hMAO-A and 4−16 μM for hMAO-B) and kurarinone (0−400 μM). The inhibition constant (K_i) was derived from the secondary plots obtained using SigmaPlot 12.0 TM software (SPCC Inc, Chicago IL, USA). Lineweaver−Burk and Dixon plots were used to determine the mode of enzyme inhibition.

5.5. Homology Modeling. The primary sequence for hD_1R was retrieved from the UniProt database having the IDs P21728 (DRD1_HUMAN). The template of the β_2 adrenergic receptor (β_2R) crystal structure with PBD ID 2RH1 was used for modeling of hD_1R using Swiss-Model server because high sequence similarity is found in the overall structure and binding sites between D_1R and β_2R.[68,69] The homology model was refined using ModRefiner server.[70]

5.6. Molecular Docking. AutoDock 4.2 program was run to conduct molecular docking and gain insights into the intermolecular interactions between kurarinone/reference ligands and receptors/enzymes.[71] X-ray crystallographic structures with PBD IDs 6CM4, 5WIV, 2BXR, and 2V60 for $hD_{2L}R$, hD_4R, hMAO-A, and hMAO-B, respectively, were used. The 3D chemical structure of kurarinone was attained from the PubChem compound database with CID 11982640. Likewise, crystal structures of L-deprenyl, clorgyline, harmine, 7-[(3-chlorobenzyl)oxy]-2-oxo-2H-chromene-4-carbaldehyde (C-17), DA, SCH23390, risperidone, butaclamol, and nemonapride were also acquired from PubChem database with CIDs 5195, 4380, 5280953, 16750123, 681, 5018, 5073, 37461, and 156333, respectively. Discovery Studio (v17.2, Accelrys, San Diego, USA) was used for enzyme/receptor preparation. AutoDockTool was employed for docking simulation and analyzing Autodock dockings by adding necessary parameters such as H-bonds, Gasteiger charge, and rotatable bonds. Grid maps were calculated using AutoGrid.

https://doi.org/10.1021/acsomega.1c04109
ACS Omega 2021, 6, 33443−33453

The grid points were generated automatically by centering on ligands (co-crystallized/reference), and the grid box was 60 × 60 × 60. Initially, the co-crystallized ligands were redocked with the proteins, and at the lowest binding energy, their binding interactions were found similar to the original PDB protein−ligand interactions to verify the docking protocol. A total of 10 independent genetic algorithms were set as docking protocols for the rigid as well as flexible ligand docking. The docking results were evaluated by AutoDockTools and visualized using Discovery Studio. The generic residue numbers (Ballesteros-Weinstein numbers) for interacting residues of DARs were obtained from the GPCR database system (https://gpcrdb.org).[72]

5.7. Drug-Likeliness and ADME Prediction. The absorption, distribution, metabolism, elimination, toxicity, and drug-likeliness characters of kurarinone were estimated by employing PreADMET (http://preadmet.bmdrc.org). Pharmacokinetic parameters, viz., lipophilicity (log *Po*/w), human intestinal absorption (HIA), plasma protein binding (PPB), and permeation across the BBB were also predicted.

■ ASSOCIATED CONTENT

Supporting Information

The Supporting Information is available free of charge at https://pubs.acs.org/doi/10.1021/acsomega.1c04109.

> Binding energies and interacting residues of kurarinone and reference ligands in the binding site of human DA (hD1, hD2L, and hD4) eeceptors; kinetic constants and inhibition mode of kurarinone for the inhibition of hMAO-A and hMAO-B; binding energies and interacting residues of kurarinone and reference ligands in hMAO-A and hMAO-B; Lineweaver−Burk and Dixon plots for the inhibition of hMAO-A and hMAO-B by kurarinone, respectively, and secondary plots for the inhibition of hMAO-B by kurarinone; molecular docking of kurarinone (red stick), harmine (HRM, blue stick), and deprenyl (black stick) with hMAO-A, zoom-in view of the ligand-binding site of hMAO-A, two-dimensional representation of interactions of kurarinone with the catalytic site residues of hMAO-A, and structure of cofactor FAD is shown using a cyan blue stick; and molecular docking of kurarinone (red stick), C17 (pink stick), and deprenyl (black stick) with hMAO-B, zoom-in view of catalytic and allosteric binding sites of hMAO-B, and two-dimensional representation of interactions of kurarinone with the catalytic and allosteric site residues of hMAO-B (PDF)

■ AUTHOR INFORMATION

Corresponding Authors

Hyun Ah Jung − *Department of Food Science and Human Nutrition, Jeonbuk National University, Jeonju 54896, Republic of Korea*; Phone: +82-63-270-4882; Email: jungha@jbnu.ac.kr

Jae Sue Choi − *Department of Food and Life Science, Pukyong National University, Busan 48513, Republic of Korea*; orcid.org/0000-0001-9034-8868; Phone: +82-51-629-7547; Email: choijs@pknu.ac.kr

Authors

Ritu Prajapati − *Department of Food and Life Science, Pukyong National University, Busan 48513, Republic of Korea*

Su Hui Seong − *Department of Food and Life Science, Pukyong National University, Busan 48513, Republic of Korea; Natural Products Research Division, Honam National Institute of Biological Resource, Mokpo 58762, Republic of Korea*

Pradeep Paudel − *Department of Food and Life Science, Pukyong National University, Busan 48513, Republic of Korea; National Center for Natural Products Research, The University of Mississippi, Oxford, Mississippi 38677, United States*; orcid.org/0000-0001-8482-1129

Se Eun Park − *Department of Food and Life Science, Pukyong National University, Busan 48513, Republic of Korea; Department of Biomedical Science, Asan Medical Institute of Convergence Science and Technology, Seoul 05505, Republic of Korea*

Complete contact information is available at: https://pubs.acs.org/10.1021/acsomega.1c04109

Author Contributions

Bioassays and original draft preparation, R.P.; molecular docking studies, S.H.S. and S.E.P.; writing—review and edit, P.P.; and study plan, design, and supervision, H.A.J. and J.S.C. All authors read and approved the final version of the paper.

Notes

The authors declare no competing financial interest.

■ ACKNOWLEDGMENTS

This research was funded by the National Research Foundation of Korea (NRF) grant funded by the Ministry of Science and ICT (no. 2020R1C1C1008331) and by the Basic Science Research Program through the National Research Foundation of Korea (NRF) funded by the Ministry of Science (2019R1I1A3A01049380).

■ REFERENCES

(1) Heng, B. C.; Aubel, D.; Fussenegger, M. An overview of the diverse roles of G-protein coupled receptors (GPCRs) in the pathophysiology of various human diseases. *Biotechnol. Adv.* **2013**, *31*, 1676−1694.

(2) Huang, Y.; Todd, N.; Thathiah, A. The role of GPCRs in neurodegenerative diseases: avenues for therapeutic intervention. *Curr. Opin. Pharmacol.* **2017**, *32*, 96−110.

(3) Hauser, A. S.; Attwood, M. M.; Rask-Andersen, M.; Schiöth, H. B.; Gloriam, D. E. Trends in GPCR drug discovery: new agents, targets and indications. *Nat. Rev. Drug Discovery* **2017**, *16*, 829−842.

(4) Jaber, M.; Robinson, S. W.; Missale, C.; Caron, M. G. Dopamine receptors and brain function. *Neuropharmacology* **1996**, *35*, 1503−1519.

(5) Rangel-Barajas, C.; Coronel, I.; Florán, B. Dopamine receptors and neurodegeneration. *Aging Dis.* **2015**, *6*, 349.

(6) Mishra, A.; Singh, S.; Shukla, S. Physiological and functional basis of dopamine receptors and their role in neurogenesis: possible implication for Parkinson's disease. *J. Exp. Neurosci.* **2018**, *12*, 1179069518779829.

(7) Frechilla, D.; Cobreros, A.; Saldise, L.; Moratalla, R.; Insausti, R.; Luquin, M.-R.; Del Río, J. n. Serotonin 5-HT1A receptor expression is selectively enhanced in the striosomal compartment of chronic parkinsonian monkeys. *Synapse* **2001**, *39*, 288−296.

(8) Vidal, B.; Sebti, J.; Verdurand, M.; Fieux, S.; Billard, T.; Streichenberger, N.; Troakes, C.; Newman-Tancredi, A.; Zimmer, L.

Agonist and antagonist bind differently to 5-HT1A receptors during Alzheimer's disease: a post-mortem study with PET radiopharmaceuticals. *Neuropharmacology* **2016**, *109*, 88−95.
(9) Shimizu, S.; Ohno, Y. Improving the treatment of Parkinson's disease: A novel approach by modulating 5-HT1A receptors. *Aging Dis.* **2013**, *4*, 1.
(10) Egashira, N.; Tanoue, A.; Matsuda, T.; Koushi, E.; Harada, S.; Takano, Y.; Tsujimoto, G.; Mishima, K.; Iwasaki, K.; Fujiwara, M. Impaired social interaction and reduced anxiety-related behavior in vasopressin V_{1A} receptor knockout mice. *Behav. Brain Res.* **2007**, *178*, 123−127.
(11) Bielsky, I. F.; Hu, S.-B.; Szegda, K. L.; Westphal, H.; Young, L. J. Profound impairment in social recognition and reduction in anxiety-like behavior in vasopressin V1a receptor knockout mice. *Neuropsychopharmacology* **2004**, *29*, 483−493.
(12) Naoi, M.; Maruyama, W. Monoamine oxidase inhibitors as neuroprotective agents in age-dependent neurodegenerative disorders. *Curr. Pharm. Des.* **2010**, *16*, 2799−2817.
(13) Jung, H. A.; Jeong, D.-M.; Chung, H. Y.; Lim, H. A.; Kim, J. Y.; Yoon, N. Y.; Choi, J. S. Re-evaluation of the antioxidant prenylated flavonoids from the roots of Sophora flavescens. *Biol. Pharm. Bull.* **2008**, *31*, 908−915.
(14) Jung, H. A.; Yoon, N. Y.; Kang, S. S.; Kim, Y. S.; Choi, J. S. Inhibitory activities of prenylated flavonoids from Sophora flavescens against aldose reductase and generation of advanced glycation endproducts. *J. Pharm. Pharmacol.* **2008**, *60*, 1227−1236.
(15) Hwang, J.-S.; Lee, S. A.; Hong, S. S.; Lee, K. S.; Lee, M. K.; Hwang, B. Y.; Ro, J. S. Monoamine oxidase inhibitory components from the roots of Sophora flavescens. *Arch. Pharmacal Res.* **2005**, *28*, 190−194.
(16) Jung, H. A.; Yokozawa, T.; Kim, B.-W.; Jung, J. H.; Choi, J. S. Selective inhibition of prenylated flavonoids from Sophora flavescens against BACE1 and cholinesterases. *Am. J. Chin. Med.* **2010**, *38*, 415−429.
(17) Jeong, G.-S.; Li, B.; Lee, D.-S.; Byun, E.; An, R.-B.; Pae, H.-O.; Chung, H.-T.; Youn, K.-H.; Kim, Y.-C. Lavandulyl flavanones from Sophora flavescens protect mouse hippocampal cells against glutamate-induced neurotoxicity via the induction of heme oxygenase-1. *Biol. Pharm. Bull.* **2008**, *31*, 1964−1967.
(18) Weng, Z.; Zeng, F.; Zhu, Z.; Qian, D.; Guo, S.; Wang, H.; Duan, J.-a. Comparative analysis of sixteen flavonoids from different parts of Sophora flavescens Ait. by ultra high-performance liquid chromatography−tandem mass spectrometry. *J. Pharm. Biomed. Anal.* **2018**, *156*, 214−220.
(19) Xie, L.; Gong, W.; Chen, J.; Xie, H.-w.; Wang, M.; Yin, X.-p.; Wu, W. The flavonoid kurarinone inhibits clinical progression of EAE through inhibiting Th1 and Th17 cell differentiation and proliferation. *Int. Immunopharmacol.* **2018**, *62*, 227−236.
(20) Yang, X.; Baburin, I.; Plitzko, I.; Hering, S.; Hamburger, M. HPLC-based activity profiling for $GABA_A$ receptor modulators from the traditional Chinese herbal drug Kushen (Sophora flavescens root). *Mol. Diversity* **2011**, *15*, 361−372.
(21) Goffin, D.; Aarum, J.; Schroeder, J. E.; Jovanovic, J. N.; Chuang, T. T. D1-like dopamine receptors regulate $GABA_A$ receptor function to modulate hippocampal neural progenitor cell proliferation. *J. Neurochem.* **2008**, *107*, 964−975.
(22) Sheng, H.-Y.; Qu, C.-L.; Huo, F.-Q.; Du, J.-Q.; Tang, J.-S. D2-like but not D1-like dopamine receptors are involved in the ventrolateral orbital cortex-induced antinociception: a GABAergic modulation mechanism. *Eur. Neurol.* **2009**, *215*, 128−134.
(23) Lee, H. W.; Ryu, H. W.; Kang, M.-G.; Park, D.; Oh, S.-R.; Kim, H. Potent Selective Monoamine Oxidase B Inhibition by Maackiain, a Pterocarpan from the Roots of Sophora flavescens. *Bioorg. Med. Chem. Lett.* **2016**, *26*, 4714−4719.
(24) Newman-Tancredi, A.; Cussac, D.; Quentric, Y.; Touzard, M.; Verrièle, L.; Carpentier, N.; Millan, M. J. Differential actions of antiparkinson agents at multiple classes of monoaminergic receptor. III. Agonist and antagonist properties at serotonin, 5-HT1 and 5-HT2, receptor subtypes. *J. Pharmacol. Exp. Ther.* **2002**, *303*, 815−822.
(25) Ge, H.; Zhang, Y.; Yang, Z.; Qiang, K.; Chen, C.; Sun, L.; Chen, M.; Zhang, J. Chemical synthesis, microbial transformation and biological evaluation of tetrahydroprotoberberines as dopamine D1/D2 receptor ligands. *Bioorg. Med. Chem.* **2019**, *27*, 2100−2111.
(26) Geha, R. M.; Chen, K.; Wouters, J.; Ooms, F.; Shih, J. C. Analysis of conserved active site residues in monoamine oxidase A and B and their three-dimensional molecular modeling. *J. Biol. Chem.* **2002**, *277*, 17209−17216.
(27) De Colibus, L.; Li, M.; Binda, C.; Lustig, A.; Edmondson, D. E.; Mattevi, A. Three-dimensional structure of human monoamine oxidase A (MAO-A): relation to the structures of rat MAO-A and human MAO-B. *Proc. Natl. Acad. Sci. U.S.A.* **2005**, *102*, 12684−12689.
(28) Son, S.-Y.; Ma, J.; Kondou, Y.; Yoshimura, M.; Yamashita, E.; Tsukihara, T. Structure of human monoamine oxidase A at 2.2-Å resolution: the control of opening the entry for substrates/inhibitors. *Proc. Natl. Acad. Sci. U.S.A.* **2008**, *105*, 5739−5744.
(29) Lipinski, C. A. Lead-and drug-like compounds: the rule-of-five revolution. *Drug Discovery Today: Technol.* **2004**, *1*, 337−341.
(30) Devi, S.; Kumar, V.; Singh, S. K.; Dubey, A. K.; Kim, J.-J. Flavonoids: Potential candidates for the treatment of neurodegenerative disorders. *Biomedicines* **2021**, *9*, 99.
(31) Grosso, C.; Valentão, P.; Ferreres, F.; Andrade, P. The use of flavonoids in central nervous system disorders. *Curr. Med. Chem.* **2013**, *20*, 4694−4719.
(32) Zheng, M.; Fan, Y.; Shi, D.; Liu, C. Antidepressant-like effect of flavonoids extracted from Apocynum venetum leaves on brain monoamine levels and dopaminergic system. *J. Ethnopharmacol.* **2013**, *147*, 108−113.
(33) Yoshitake, T.; Yoshitake, S.; Kehr, J. The Ginkgo biloba extract EGb 761® and its main constituent flavonoids and ginkgolides increase extracellular dopamine levels in the rat prefrontal cortex. *Br. J. Pharmacol.* **2010**, *159*, 659−668.
(34) Butterweck, V.; Nahrstedt, A.; Evans, J.; Hufeisen, S.; Rauser, L.; Savage, J.; Popadak, B.; Ernsberger, P.; Roth, B. L. In vitro receptor screening of pure constituents of St. John's wort reveals novel interactions with a number of GPCRs. *Psychopharmacology* **2002**, *162*, 193−202.
(35) Park, S. E.; Paudel, P.; Wagle, A.; Seong, S. H.; Kim, H. R.; Fauzi, F. M.; Jung, H. A.; Choi, J. S. Luteolin, a Potent Human Monoamine Oxidase-A Inhibitor and Dopamine D4 and Vasopressin V1A Receptor Antagonist. *J. Agric. Food Chem.* **2020**, *68*, 10719−10729.
(36) Yap, B. K.; Buckle, M. J. C.; Doughty, S. W. Homology modeling of the human $5\text{-}HT_{1A}$, $5\text{-}HT_{2A}$, D_1, and D_2 receptors: model refinement with molecular dynamics simulations and docking evaluation. *J. Mol. Model.* **2012**, *18*, 3639−3655.
(37) Tomic, M.; Seeman, P.; George, S. R.; Odowd, B. F. Dopamine D_1 receptor mutagenesis: role of amino acids in agonist and antagonist binding. *Biochem. Biophys. Res. Commun.* **1993**, *191*, 1020−1027.
(38) Wang, S.; Che, T.; Levit, A.; Shoichet, B. K.; Wacker, D.; Roth, B. L. Structure of the D_2 dopamine receptor bound to the atypical antipsychotic drug risperidone. *Nature* **2018**, *555*, 269−273.
(39) Kalani, M. Y. S.; Vaidehi, N.; Hall, S. E.; Trabanino, R. J.; Freddolino, P. L.; Kalani, M. A.; Floriano, W. B.; Kam, V. W. T.; Goddard, W. A. The predicted 3D structure of the human D_2 dopamine receptor and the binding site and binding affinities for agonists and antagonists. *Proc. Natl. Acad. Sci. U.S.A.* **2004**, *101*, 3815−3820.
(40) Ledonne, A.; Mercuri, N. B. Current concepts on the physiopathological relevance of dopaminergic receptors. *Front. Cell. Neurosci.* **2017**, *11*, 27.
(41) Hall, E. D.; Andrus, P. K.; Oostveen, J. A.; Althaus, J. S.; Von Voigtlander, P. F. Neuroprotective effects of the dopamine D_2/D_3 agonist pramipexole against postischemic or methamphetamine-induced degeneration of nigrostriatal neurons. *Brain Res.* **1996**, *742*, 80−88.

https://doi.org/10.1021/acsomega.1c04109
ACS Omega 2021, 6, 33443−33453

(42) O'Neill, M. J.; Hicks, C. A.; Ward, M. A.; Cardwell, G. P.; Reymann, J.-M.; Allain, H.; Bentué-Ferrer, D. Dopamine D_2 receptor agonists protect against ischaemia-induced hippocampal neurodegeneration in global cerebral ischaemia. *Eur. J. Pharmacol.* **1998**, *352*, 37−46.
(43) Chen, S.; Zhang, X.; Yang, D.; Du, Y.; Li, L.; Li, X.; Ming, M.; Le, W. D_2/D_3 receptor agonist ropinirole protects dopaminergic cell line against rotenone-induced apoptosis through inhibition of caspase- and JNK-dependent pathways. *FEBS Lett.* **2008**, *582*, 603−610.
(44) Van Kampen, J. M.; Eckman, C. B. Dopamine D_3 receptor agonist delivery to a model of Parkinson's disease restores the nigrostriatal pathway and improves locomotor behavior. *J. Neurosci.* **2006**, *26*, 7272−7280.
(45) Hitchcott, P. K.; Bonardi, C. M. T.; Phillips, G. D. Enhanced stimulus-reward learning by intra-amygdala administration of a D_3 dopamine receptor agonist. *Psychopharmacology* **1997**, *133*, 240−248.
(46) Bernaerts, P.; Tirelli, E. Facilitatory effect of the dopamine D_4 receptor agonist PD168, 077 on memory consolidation of an inhibitory avoidance learned response in C57BL/6J mice. *Behav. Brain Res.* **2003**, *142*, 41−52.
(47) Powell, S.; Paulus, M. P.; Hartman, D. S.; Godel, T.; Geyer, M. A. RO-10-5824 is a selective dopamine D_4 receptor agonist that increases novel object exploration in C57 mice. *Neuropharmacology* **2003**, *44*, 473−481.
(48) Woolley, M. L.; Waters, K. A.; Reavill, C.; Bull, S.; Lacroix, L. P.; Martyn, A. J.; Hutcheson, D. M.; Valerio, E.; Bate, S.; Jones, D. N. C.; Dawson, L. A. Selective dopamine D_4 receptor agonist (A-412997) improves cognitive performance and stimulates motor activity without influencing reward-related behaviour in rat. *Behav. Pharmacol.* **2008**, *19*, 765−776.
(49) Pan, X.; Kaminga, A. C.; Wen, S. W.; Wu, X.; Acheampong, K.; Liu, A. Dopamine and dopamine receptors in Alzheimer's disease: a systematic review and network meta-analysis. *Front. Aging Neurosci.* **2019**, *11*, 175.
(50) Lebel, M.; Patenaude, C.; Allyson, J.; Massicotte, G.; Cyr, M. Dopamine D1 receptor activation induces tau phosphorylation via cdk5 and GSK3 signaling pathways. *Neuropharmacology* **2009**, *57*, 392−402.
(51) Lud Cadet, J.; Jayanthi, S.; T. McCoy, M.; Beauvais, G.; Sheng Cai, N. Dopamine D1 receptors, regulation of gene expression in the brain, and neurodegeneration. *CNS Neurol. Disord.: Drug Targets* **2010**, *9*, 526−538.
(52) Wersinger, C.; Chen, J.; Sidhu, A. Bimodal induction of dopamine-mediated striatal neurotoxicity is mediated through both activation of D_1 dopamine receptors and autoxidation. *Mol. Cell. Neurosci.* **2004**, *25*, 124−137.
(53) Feyder, M.; Bonito-Oliva, A.; Fisone, G. L-DOPA-induced dyskinesia and abnormal signaling in striatal medium spiny neurons: focus on dopamine D_1 receptor-mediated transmission. *Front. Behav. Neurosci.* **2011**, *5*, 71.
(54) Lanza, K.; Meadows, S. M.; Chambers, N. E.; Nuss, E.; Deak, M. M.; Ferré, S.; Bishop, C. Behavioral and cellular dopamine D1 and D3 receptor-mediated synergy: Implications for L-DOPA-induced dyskinesia. *Neuropharmacology* **2018**, *138*, 304−314.
(55) Aubert, I.; Guigoni, C.; Håkansson, K.; Li, Q.; Dovero, S.; Barthe, N.; Bioulac, B. H.; Gross, C. E.; Fisone, G.; Bloch, B.; Bezard, E. Increased D1 dopamine receptor signaling in levodopa-induced dyskinesia. *Ann. Neurol.* **2005**, *57*, 17−26.
(56) Grondin, R.; Doan, V. D.; Grégoire, L.; Bédard, P. J. D1 receptor blockade improves L-dopa−induced dyskinesia but worsens parkinsonism in MPTP monkeys. *Neurology* **1999**, *52*, 771.
(57) Qin, Y.; Zhu, Y.; Xue, X.; Zhou, G.; Li, H.; Wang, J. An In Vitro Study for Evaluating Permeability and Metabolism of Kurarinone. *Evidence-Based Complementary Altern. Med.* **2020**, *2020*, 5267684.
(58) Huang, Y.; Lin, H.; Chen, Y.; Huang, X. Pharmacokinetic and bioavailability study of kurarinone in dog plasma by UHPLC−MS/MS. *Biomed. Chromatogr.* **2020**, *34*, No. e4945.
(59) Jiang, P.; Zhang, X.; Huang, Y.; Cheng, N.; Ma, Y. Hepatotoxicity induced by Sophora flavescens and hepatic accumulation of kurarinone, a major hepatotoxic constituent of Sophora flavescens in rats. *Molecules* **2017**, *22*, 1809.
(60) Yu, Q.; Cheng, N.; Ni, X. Identifying 2 prenylflavanones as potential hepatotoxic compounds in the ethanol extract of Sophora flavescens. *J. Food Sci.* **2013**, *78*, T1830−T1834.
(61) Nishikawa, S.; Inoue, Y.; Hori, Y.; Miyajima, C.; Morishita, D.; Ohoka, N.; Hida, S.; Makino, T.; Hayashi, H. Anti-Inflammatory Activity of Kurarinone Involves Induction of HO-1 via the KEAP1/Nrf2 Pathway. *Antioxidants* **2020**, *9*, 842.
(62) Zhang, X.; Jiang, P.; Chen, P.; Cheng, N. Metabolism of kurarinone by human liver microsomes and its effect on cytotoxicity. *Pharm. Biol.* **2016**, *54*, 619−627.
(63) Youdim, M. B. H. Why do we need multifunctional neuroprotective and neurorestorative drugs for Parkinson's and Alzheimer's diseases as disease modifying agents. *Exp. Neurobiol.* **2010**, *19*, 1.
(64) Chen, X.-W.; Sun, Y.-Y.; Fu, L.; Li, J.-Q. Synthesis and pharmacological characterization of novel N-(trans-4-(2-(4-(benzo[d] isothiazol-3-yl) piperazin-1-yl) ethyl) cyclohexyl) amides as potential multireceptor atypical antipsychotics. *Eur. J. Med. Chem.* **2016**, *123*, 332−353.
(65) Gorbunov, E.; Ertuzun, I.; Kachaeva, E.; Tarasov, S.; Epstein, O. In vitro screening of major neurotransmitter systems possibly involved in the mechanism of action of antibodies to S100 protein in released-active form. *Neuropsychiatr. Dis. Treat.* **2015**, *11*, 2837.
(66) Paudel, P.; Seong, S. H.; Park, S. E.; Ryu, J. H.; Jung, H. A.; Choi, J. S. In vitro and in silico characterization of G-protein coupled receptor (GPCR) targets of phlorofucofuroeckol-A and dieckol. *Mar. Drugs* **2021**, *19*, 326.
(67) Prajapati, R.; Park, S. E.; Park, H. J.; Jung, H. A.; Choi, J. S. Identification of a potent and selective human monoamine oxidase-A inhibitor, glycitein, an isoflavone isolated from Pueraria lobata flowers. *ACS Food Sci. Technol.* **2021**, *1*, 538−550.
(68) Kołaczkowski, M.; Bucki, A.; Feder, M.; Pawłowski, M. Ligand-optimized homology models of D_1 and D_2 dopamine receptors: Application for virtual screening. *J. Chem. Inf. Model.* **2013**, *53*, 638−648.
(69) Guex, N.; Peitsch, M. C.; Schwede, T. Automated comparative protein structure modeling with SWISS-MODEL and Swiss-PdbViewer: A historical perspective. *Electrophoresis* **2009**, *30*, S162−S173.
(70) Xu, D.; Zhang, Y. Improving the physical realism and structural accuracy of protein models by a two-step atomic-level energy minimization. *Biophys. J.* **2011**, *101*, 2525−2534.
(71) Goodsell, D. S.; Morris, G. M.; Olson, A. J. Automated docking of flexible ligands: applications of AutoDock. *J. Mol. Recognit.* **1996**, *9*, 1−5.
(72) Kooistra, A. J.; Mordalski, S.; Pándy-Szekeres, G.; Esguerra, M.; Mamyrbekov, A.; Munk, C.; Keserű, G. M.; Gloriam, D. E. GPCRdb in 2021: integrating GPCR sequence, structure and function. *Nucleic Acids Res.* **2021**, *49*, D335−D343.

https://doi.org/10.1021/acsomega.1c04109
ACS Omega 2021, 6, 33443−33453